SIMULATION OF GAS LEAKAGE ON BALL SEAT VALVES

Felix Fischer[1]*, Katharina Schmitz[1]

[1]*Institute for Fluid Power Drives and Systems, Campus-Boulevard 30, 52074 Aachen*

* Corresponding author: Tel.: +49 241 80-47725; E-mail address: f.fischer@ifas.rwth-aachen.de

ABSTRACT

Gas leakage is a critical issue in various industrial applications that utilize ball seat valves. This is especially relevant for hydrogen applications, due to its high reactivity. This paper presents the application of a model for analyzing liquid leakage on ball seat valves applied to gases and the experimental validation of these results. The research objective is to enhance the understanding of the leakage mechanisms and provide valuable insights for improving the design and performance of ball seat valves. The simulation model considers valve geometry, surface roughness, and material properties to predict the leakage behavior accurately. The simulation method is based on the contact mechanics model developed by Persson [1]. It considers the surface roughness via the two-dimensional spectral density. The model is validated experimentally by comparing the simulated leakage rates with experimentally measured values for seats with different surface roughness and anisotropy. This way, the validation shows whether the leakage model can be applied to gases.

Keywords: Simulation, Leakage, Tribology, Gas, Valves, Pneumatics

1. MOTIVATION

Metallic sealing in gas applications is a highly specialized and crucial technology known for its ability to create gas-tight seals in demanding environments. This method relies on metal-to-metal interfaces to achieve tightness, effectively preventing the escape or ingress of gases. These applications encompass various industries, including aerospace, automotive, petrochemical, and power generation, playing a pivotal role in ensuring safety and operational reliability.

One notable advantage of metallic sealing is its capability to achieve hermetic tightness, which is essential in applications where gas leakage is unacceptable, such as in spacecraft, vacuum chambers, and certain industrial processes. Furthermore, these seals demonstrate exceptional resistance to corrosion, temperature and chemical exposure, making them suitable for environments where gases may be corrosive or chemically reactive. In addition to their longevity and reliability, metallic seals have a longer service life compared to many other sealing methods, reducing maintenance and replacement costs.

In the hydrogen industry, the advantages of metallic sealing are particularly noteworthy. Given the unique properties and challenges associated with hydrogen gas, metallic seals offer a reliable solution. Hydrogen is known for its small molecular size, which allows it to permeate through materials that might be impermeable to other gases. When soft polymer seals are exposed to hydrogen, pressure changes can lead to fractures of the seals due to hydrogen contained in the material. Metallic seals, with their gas-tightness, are crucial in preventing hydrogen leakage, especially in applications involving hydrogen storage, transportation, and fuel cells [2].

Another notable aspect is the absence of PFAS (per- and poly-fluoroalkyl substances) such as PTFE (polytetrafluoroethylene) in metallic sealing. PTFE, a commonly used material in traditional gasket

seals, has come under critique recently due to its long-term chemical stability. Due to the spread of microscopic PFAS particles, residues of PFAS can be found in human bodies. Especially, a high concentration of PFOA (perfluorooctanoic acid), a PFAS used in the production of PTFE, is known to accumulate permanently in human bodies. The effects of PFAS on the environment and human health have yet to be examined [3,4].

Simulations are essential for assessing the leak tightness of metallic seals. They provide a cost-effective way to evaluate seal performance early in the design process, predict how seals will perform under various conditions, and identify potential weaknesses or areas susceptible to leaks. Simulations also help to optimize seal designs, reduce costs, and accelerate development.

The study examines the gas leakage in metallic seals, focusing on ball seat valves, see **Figure 1**, as an example. These valves serve as commonly used check valves and provide an adequate model for metallic seals due to the easy ball and seat exchange in an experimental setting. This allows for the study of the varying effects of materials and surfaces under consistent conditions. The findings and approaches outlined in this study can be applied to other configurations of metal seals.

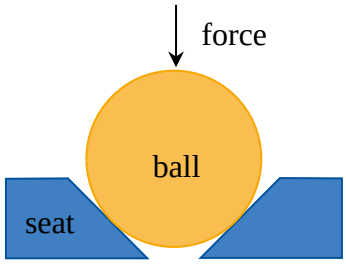

Figure 1: Sketch of a ball seat valve

The paper is structured as follows: In section 2 the state of the art of leakage simulations for metallic seals as well as for gas leakage is presented. A short introduction to the contact mechanics theory developed by Persson, on which the simulation model used in this paper is based, is given in section 3. The simulation method as well as the experimental set-up for the validation are introduced in section 4, while the results of both the simulation and experiment are discussed in section 5. This paper concludes with a summary and outlook.

2. STATE OF THE ART

Leakage simulations of metallic seals have experienced significant progress recently, covering various aspects. One noteworthy development includes a study that created an experimental setup to investigate fluid leakage in metallic seals, which specifically concentrated on water leakage between a steel sphere and a steel body with a conical surface. The experimental findings align well with a corresponding theoretical model, which predicts that plastic deformations may reduce the leak rate by a factor of about 8 [5,6].

In another study, Zhang et al. analyzed fluid leak rates across metal sealing surfaces by creating fractal models for both the contact and leakage processes. They refined the model to describe the seal-contact interface of two metal rough surfaces. In this study, the authors used fractal theory to mathematically model the leakage channel under the contact surface. They also analyzed how factors such as fractal structure, surface material, and gasket size affect the contact and leakage processes. To simulate sealed ring gaskets, numerical simulations were used [7].

Additionally, in another study, Tikhomorov, Gorlenko, and Izmerov used a mathematical modeling approach to simulate leakage through mechanical seals, accounting for waviness and roughness by treating the microscopic net of flow channels through the contact area as a porous medium [8].

These advancements contribute to better comprehension and improved predictive abilities for administering leakage in metallic seals.

The leak tightness of seals against gaseous media has not yet been studied widely. Most of the knowledge gained from research on metallic seals in general is also applicable to gases, but there are still some relevant differences.

A study calculated the leakage in gas labyrinth seals compared to the leakage for liquids. The research revealed that bulk-flow models (BFMs) for gas labyrinth seals often inaccurately predict mass flow. Labyrinth seal mass flow prediction was analyzed using computational fluid dynamics (CFD) to evaluate the effects of tip clearance and operating conditions, and an updated kinetic energy transfer coefficient was derived from the data to improve the accuracy of the Neumann leakage equation.

In another paper, Huon et al. analyzed the gas leakage for polymer seals. The leak rate depends on the interfacial surface roughness and viscoelastic properties of the rubber. The authors present a theory for gas flow that considers both diffusive and ballistic flow.

In the same paper, these models have been compared to experiments. To create random surface roughness, the rubber O-rings undergo sandblasting. Notably, while gas leakage occurs, there is no such issue observed for water-filled barrels. This is attributed to capillary effects resulting from Laplace pressure or surface energy [9].

3. THEORETIC BACKGROUND

The simulation method presented in this paper is based on Persson et al.'s percolation method and contact mechanics.

This contact mechanics model is rooted in a theoretical framework that addresses the intricate dynamics of rough surfaces in contact. This model employs principles from solid mechanics and surface science, providing a comprehensive understanding of contact mechanics. At its essence, the model recognizes the intrinsic roughness of real physical surfaces by characterizing these irregularities through statistical descriptors like power spectral density (PSD) functions, usually denoted as $C(\boldsymbol{q})$, with $\boldsymbol{q}$ being the two-dimensional surface roughness wave vector [10].

Elastic deformation of the contacting materials due to an applied load is a crucial factor. To analyze this deformation, contact area, and pressure distribution, Hertzian elasticity theory is employed. The model utilizes integral equations derived from Green's function formalism to connect contact pressure, deformation, and adhesion while accounting for the nonlinearity induced by surface roughness. With this formalism, a modified contact pressure relation $p_C(u)$ can be derived, which connects the local contact pressure p_C with the average separation of the surfaces u [11].

Material properties, such as elasticity and Poisson's ratio, are crucial in characterizing how materials respond to external loads and deformations. Moreover, statistical mechanics principles are utilized to describe the distribution of contact points and the probability of adhesive interactions, which enhances the model's effectiveness in describing the macroscopic mechanical behavior of rough surfaces [10].

The leakage theory developed by Persson et al. is based on the concept of percolation theory. It treats the evolution of the pressure distribution with increasing resolution of the surface roughness as a diffusive process in which the resolution replaces the function of time. This approach allows a detailed analysis of how surface roughness affects the effective contact area and the leakage rate.

In their work, they explain the leakage mechanism of the sealing interface based on their contact mechanics theory and two-dimensional percolation theory. This theory predicts that when the relative

area ratio of the apparent and the real sealing surface Π is about 0.42, a leakage channel will be formed at the sealing interface, and the fluid will flow from the high-pressure side to the low-pressure side. In this theory, the real contact area (and accordingly Π) is not only a function of the contact pressure p_C respectively u, but also of the magnification ζ. The magnification denotes a cut-off of the PSD and it indicates up to which wave vectors q are considered in the evaluation. Hence, ζ can be treated as the resolution of the contact. The ratio Π decreases as ζ increases. This allows for the definition of a critical magnification ζ for every contact pressure, at which the contact area percolates. The theory then predicts the average separation of surfaces at a magnification slightly above this critical magnification. The leakage can then be calculated using the Bernoulli equation for a thin gap [12]. In general, the Bernoulli equation is valid for both compressible and incompressible fluids.

Alternative to the critical junction approach, which has been used in this paper, Persson et al. also propose the effective medium approach, which calculates the effective conductivity of the mesh of channels that percolate the contact area. This method reaches very similar results to the critical junction method [13]. The predictions by Persson et al.'s contact theory have been validated experimentally for liquid leakage at polymeric and metallic seals multiple times [5,14].

4. METHODOLOGY

This section introduces the methodology of the study presented in this work. It is separated into two sections. The first section introduces the simulation used for calculating the leak rate. In the second section, the test rig used for experimental validation of the simulation is presented.

In this work, a total of six different seats with varying surface properties have been analyzed simulationally and experimentally. The leakage of these valves has been evaluated for relative air pressures up to 7 bar. These are the conditions usually found in pneumatic systems.

4.1. Simulation

The simulation implemented for this work is based on the contact mechanics model by Persson et al. presented in section 3. The leakage simulation developed in this paper can be divided into two sub-steps: a microscopic and a macroscopic one.

The microscopic simulation examines the deformation of the roughness peaks and the resulting network of microscopic channels. The length and shape of these channels result from the topography of the surfaces and the contact pressure distribution determined in the macroscopic simulation using Persson contact theory. The exact surface structure is incorporated statistically in the form of the 2D power spectral density.

In the macroscopic simulation, the contact pressure distribution and thus the contact width are determined. This calculation is based on the applied pressures and forces, the geometry of the valve, and the material properties of the seat and sealing body. The simulation method is based on analytical equations for the contact pressure distribution.

To calculate the leakage, the flow through the contact area has to be determined using a flow model. For this purpose, the critical resolution method is used in this paper. Once the model has been successfully developed, the results can be validated with the measurements from the next subsection.

Surface analysis

The first step of the simulation is the microscopic analysis. In this step, the provided surfaces are analyzed and the contact pressure relation $p_C(u)$ is calculated based on these measurements. For this reason, the two-dimensional PSDs are calculated for every surface. The surface data has been

measured by optical microscopy with a vertical and lateral resolution of up to 270 nm. An estimate for the true 2D-PSD can be calculated by a two-dimensional version of Welch's method [15].

A depiction of the two-dimensional PSD of the first of the six seats can be seen in **Figure 2**. On the left, a two-dimensional representation of the upper right quadrant (all components of $\boldsymbol{q}$ are positive) of the PSD can be seen. On the right-hand side, the comparison of the PSD in the direction of the fluid leakage, the radial direction, and the azimuthal (tangential) direction, which is orthogonal to the radial direction (direction of fluid flow), is shown.

Based on the two-dimensional PSD, it is possible to calculate the radially averaged PSD $C(q)$, as well as the Peklenik number γ, which represents the degree of the anisotropy. In general, γ will be a function of ζ [16]. The exact value of γ is dependent on the orientation of the surface. In this work, the local orthonormal coordinate system is chosen, such that the x-axis aligns with the radial direction of the seat. Thus, a value of γ below indicates, that the surface asperities are mainly aligned in the azimuthal direction. This is very typical for technical surfaces of seats because they are usually manufactured by turning and the primary contribution to the roughness are the grooves left over by this manufacturing process. The remains of these grooves can usually even be seen after post-processing

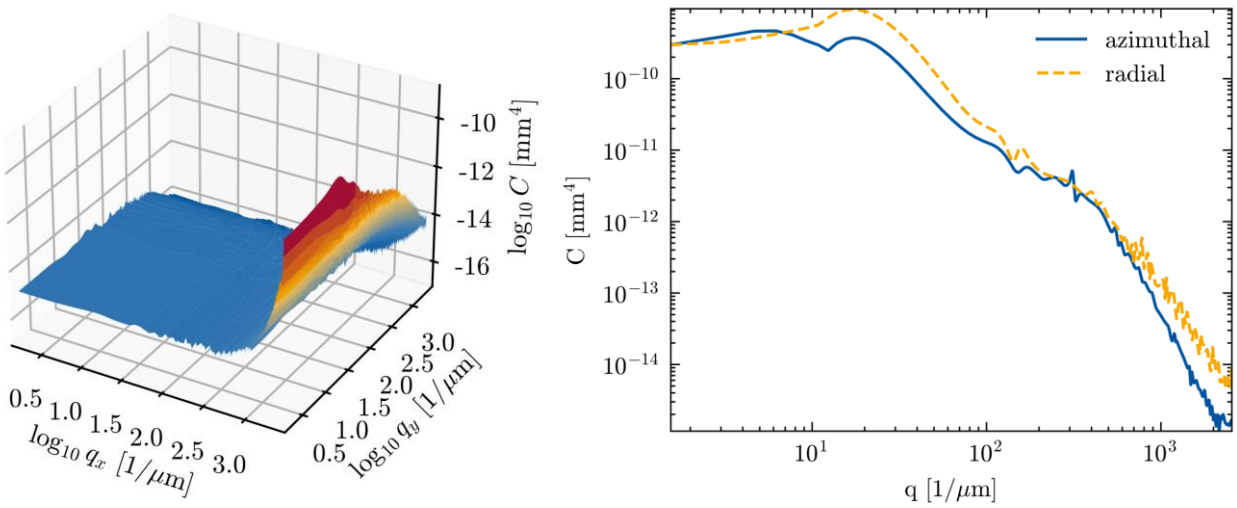

Figure 2: Two-dimensional PSD of seat 1

The two most important variables to describe the roughness of any given surface are the two-dimensional root mean square roughness S_Q and the Peklenik number γ. Both can be calculated either directly from the surface topography in spatial coordinates or from the two-dimensional PSD in the wave vector space. The consistency of the PSD calculation can be verified by comparing the results of both calculations. In further evaluations of the surfaces, only $C(q)$ and $\gamma(\zeta)$ are needed.

The radially averaged PSD of seat 1, as well as the function for γ can be seen in **Figure 3**.

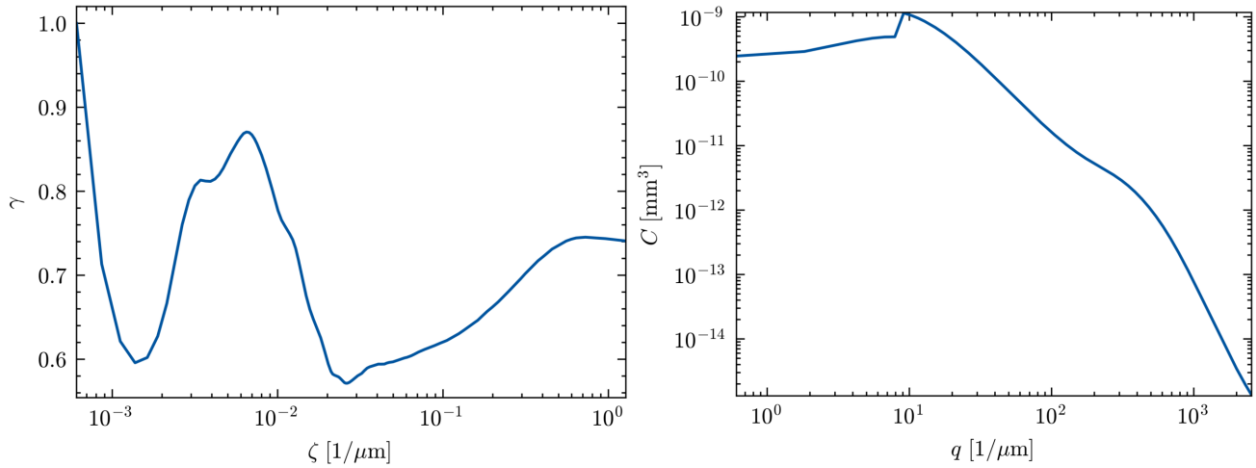

Figure 3: Radially averaged PSD and the magnification-dependent Peklenik number of seat 1

The values of S_Q and γ (= $\gamma(q_{max})$) of the surfaces analyzed in this work are listed in **Table 1**.

Table 1: Properties of the surfaces

Measured surface	S_Q [µm]	γ	Measured surface	S_Q [µm]	γ
Seat 1	2.5	0.74	Seat 4	1.6	0.50
Seat 2	2.7	0.94	Seat 5	1.0	0.52
Seat 3	5.2	0.40	Seat 6	1.9	0.39

Using these PSDs, it is possible to calculate the contact pressure distribution p_C and the fraction of the real contact area Π as a function of ζ for all contact pressures for each surface. In **Figure 4**, graphs of these quantities for seat 1 can be seen. The ratio Π is depicted for a contact pressure of 55 MPa.

Based on these prerequisites, it is possible to calculate the pressure flow factors ϕ_P and shear flow factors ϕ_S as defined by Patir and Cheng [17]. The flow factors indicate the influence of the surface roughness on the fluid dynamics as described by the average Reynolds equation. The shear flow factors indicate the amount of fluid transported in case of a relative motion of the rough surfaces, while the pressure flow factors indicate the change of the flow through the system compared to the expected flow through a smooth system with the same geometry. Patir and Cheng present in their work an approximative formula for both flow factors ϕ based only on S_Q and γ. The result flow factors differ from the results predicted by the Persson theory, which takes into account γ and $C(q)$ [18].

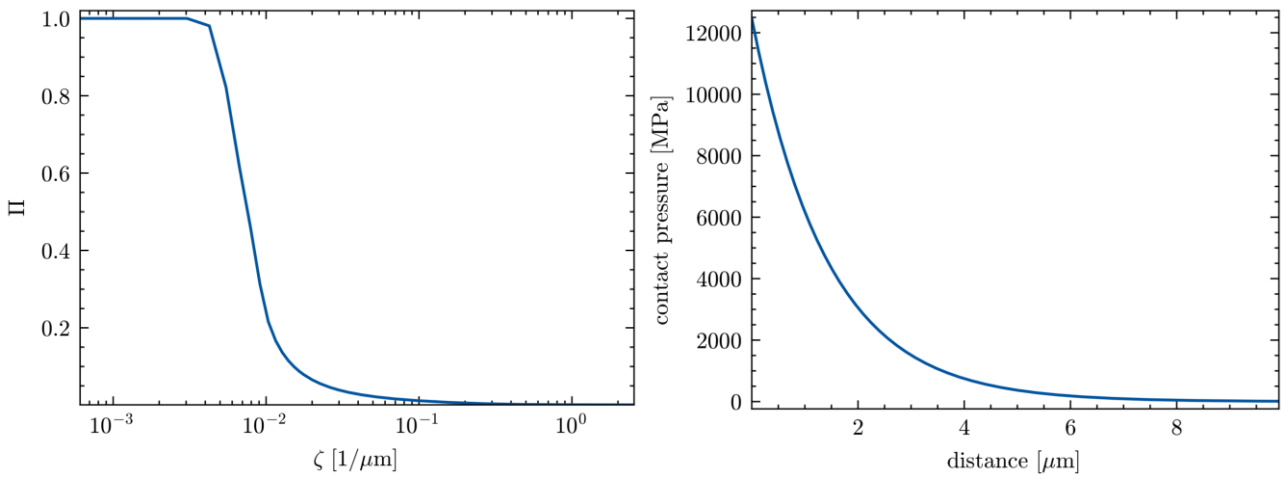

Figure 4: Ratio of real contact area vs. apparent contact area and the contact pressure relation of seat 1

A comparison between the shear flow factors and the pressure flow factors according to the Persson

theory and the approximation by Patir and Cheng can be seen in Figure 5.

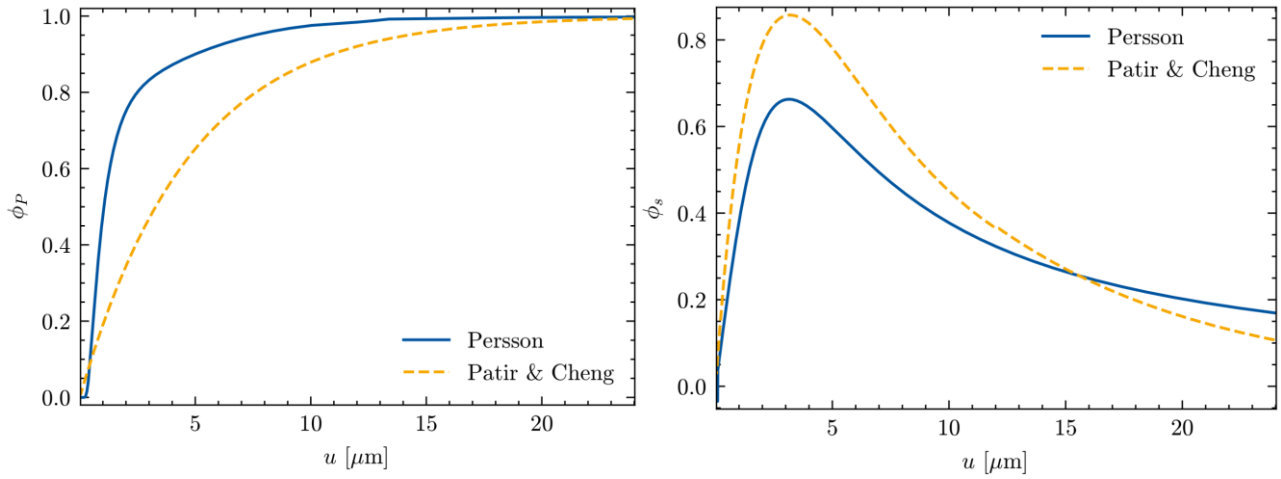

Figure 5: Pressure and shear flow factors of seat 1

In case of leakage at static ball seat valves, the shear flow factors are not needed for further calculations. However, the pressure flow factors are directly proportional to the leakage of the valve. Due to the dependence of ϕ_P on the contact pressure, which can be mapped to the distance u bijectively, as well as the dependence of the leakage on the width of the contact area, the contact pressure distribution must still be calculated. This calculation is presented in the following section.

Contact pressure distribution

The contact pressure distribution of the ball and the conical seat must be calculated based on the geometry and the material properties of the bodies at contact. These macroscopical contact properties are, however, still dependent on the microscopic contact pressure relation. The elasto-plastic contact between the ball and the seat can be separated into two different contributions. On the one hand, there is the elastic deformation of the macroscopic smooth bodies. On the other hand, there is the elasto-plastic deformation of the surface asperities. For low contact pressures, it can be assumed, that the almost whole elastic energy can be encompassed by the elastic deformation of the surface.

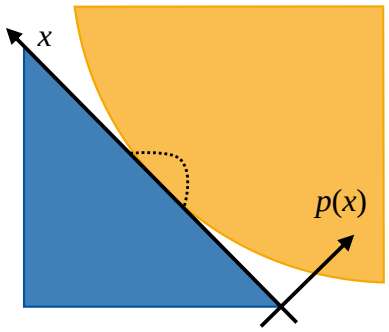

Figure 6: Coordinates used for expressing the contact pressure distribution on the seat (shown in blue)

Using this approximation, and fitting the contact pressure relation seen in **Figure 4** by an exponential function of the form $p_C(u) = p_{\max} \exp(-u/u_0)$, it is possible to calculate the contact pressure distribution analytically. The contact pressure distribution along the flank of the ball seat valve can be calculated by the following Gaussian bell curve [5]:

$$p(x) = \frac{1}{2\pi R \cos\theta \sin\theta} \frac{F}{\sqrt{2\,\pi\, R u_0}} \exp\left(-\frac{(x-x_0)^2}{2Ru_0}\right) \tag{1}$$

In this equation, F is the total normal force acting on top of the ball, R is the radius of the ball, θ is

the angle of the slope of the seat, x is the position along the slope (see **Figure 6**), and x_0 is the position of the maximum of the curve.

The geometry of the test object used in this work, as well as the material parameters, are listed in **Table 2**. The geometry and the material are equal for all seats examined in this work.

Table 2: Parameters of the test objects

Parameter of ball	Value	Parameter of seat	Value
Radius R	2 cm	Inner radius	7.5 mm
Young's modulus	190 GPa	Young's modulus	200 GPa
Poisson's ratio	0.28	Poisson's ratio	0.28
Yield strength	650 MPa	Yield strength	550 MPa
		Slope of the flank	$\pi/4$ (= 45°)

The calculated contact pressure distribution for seat 1 can be seen in **Figure 7**. Using this contact pressure relation, the maximal contact pressure can be read directly from the equation. However, the width of the contact area cannot be defined trivially. The Gaussian curve in this model does never reach zero and the areas of low contact pressure are not relevant for the seal. Thus, in this work, the contact area is arbitrarily chosen as the double standard deviation of the bell curve. This choice allows the definition of a consistent method of calculating the width based on the given parameters. Other possible choices would be, for example, the half-width height of the curve. In either case, there is a linear relation between these parameters. The width itself enters linearly into the leakage.

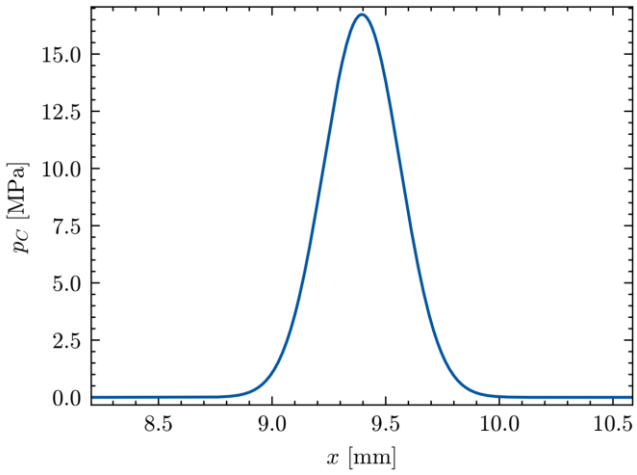

Figure 7: Pressure distribution of seat 1 at a relative gas pressure of p = 5.1 bar

The mass flow rate $\dot{m}$ can be calculated by using the following equation, based on the Hagen-Poiseuille equation for under-critical gases with constant viscosity, which is a valid approximation for air at small pressures:

$$\dot{m} = p\,\rho(p)\frac{u^3}{12\,\eta}\phi_P\frac{R\,sin\,\theta\,cos\,\theta}{a_C}$$

In this equation, p is the relative gas pressure, and a_C is the calculated width of the contact. The density ρ is, according to the ideal gas law, a function of both the pressure and the temperature. In this case, due to the small leak rate, the process is assumed to be isothermal at the environmental temperature.

With these steps, it is possible to calculate the leakage of the valves. The results of this simulation will be validated experimentally; the next section introduces the experimental setup used in this work.

4.2. Experiment

The simulation presented in this paper is validated experimentally using a test rig designed at ifas for this purpose. This test rig allows for the calculation of the leak rate by measuring the decrease of the relative pressure inside a closed cavity connected to the closed valve over time. A circuit plan of the test rig used in this work can be seen in **Figure 8**.

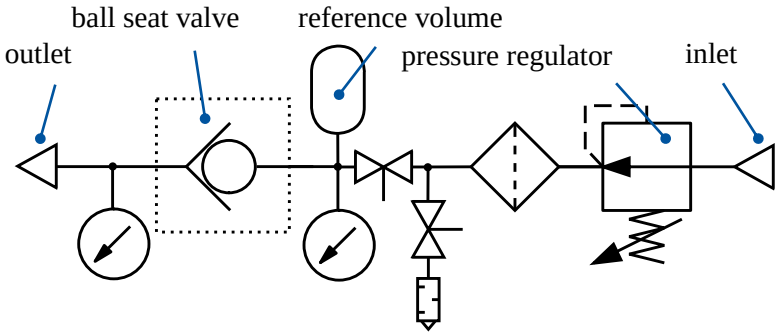

Figure 8: Circuit plan of the test rig

To measure the pressure drop-off due to the leakage through the valve correctly, it is important to ensure that the other connections to the reference volume are leak-tight compared to the seat valve. In this work, this has been assured by measuring the leak rate on a perfectly tight reference valve. The pressure drop-off has been measured five times for every seat with a new mounting process between every single measurement. The pressure curve of a single measurement on seat 5 can be seen on the left-hand side of **Figure 9**. The dotted red lines indicate the cut-offs of the evaluated time. The right-hand side shows the relation between the relative gas pressure and the mass flow rate. The relation between the mass flow rate and relative pressure can be calculated by the following formula, which can be derived from the ideal gas law:

$$\dot{m} = \frac{V}{R_s T} \frac{\mathrm{d}p}{\mathrm{d}t} \tag{2}$$

In this equation, V represents the closed reference volume, R_S is the specific gas constant of air, and T the (constant) temperature of the system.

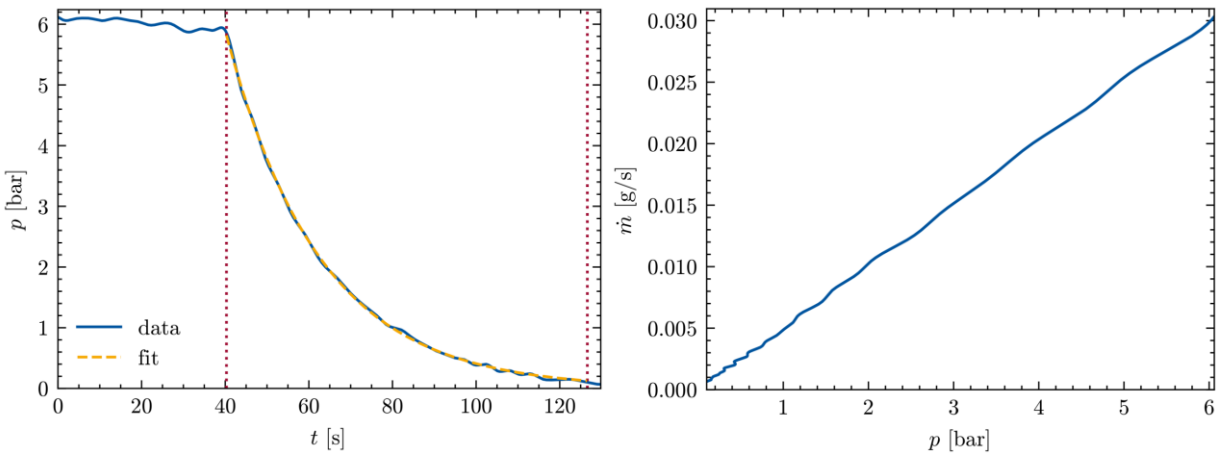

Figure 9: Pressure drop-off and leak rate of the first seat

The derivative of the pressure can be found by applying an exponential fit to the graph of *p(t)*, as seen on the left-hand side, and taking the analytical derivative of this fit. The bijective form of this relation allows for the calculation of the leak rate for every relative pressure for each measurement. Then, these results are averaged for a chosen set of relative pressures over the whole set of measurements,

and the mean, as well as the uncertainty of the leak rate, can be found.

5. RESULTS AND DISCUSSION

A comparison of the measured and the simulated leak rates can be seen in **Figure 10**. It shows the leak rates for seat 6 (left) and seat 3 (right), which have similar anisotropy, but very different roughness and different leak rates, see **Table 1**.

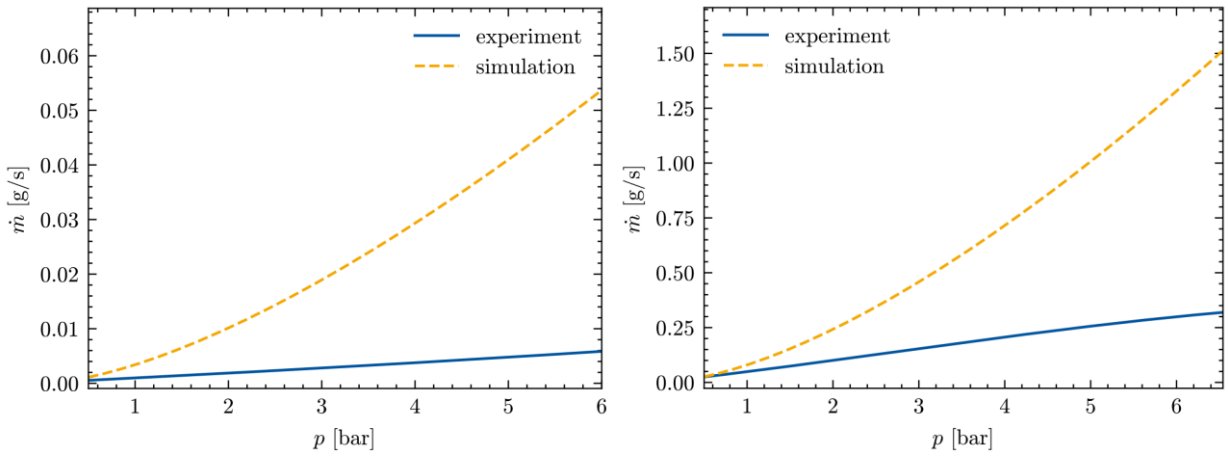

Figure 10: Comparison of the simulated and the experimental leak rates for seats 6 and 3

In both cases, the simulation overestimates the leak rate for high relative pressures and accordingly high contact pressures. In the case of seat 4 on the left-hand side, the leakage is underestimated for low gas pressures.

The simulated and measured leak rates at p = 4 bar are listed in **Table 3.**

Table 3: Leak rates at p = 4 bar

Measured surface	Simulation [mg/s]	Experiment [mg/s]	Measured surface	Simulation [mg/s]	Experiment [mg/s]
Seat 1	2.5	20.2	Seat 4	13.0	9.9
Seat 2	2.7	23.8	Seat 5	1.0	5.0
Seat 3	702.0	206.8	Seat 6	31.8	3.8

The reason for this overestimation is the flow law implemented in this simulation. The simulation tool has originally been developed for liquid leakage, rather than gas leakage. Due to the circumstances of the fluid, it could be possible, that the flow conditions are turbulent, i.e. the Reynolds number is too high, and in this case, both the flow factor method and the Hagen-Poiseuille equation are not applicable. If the diameter of the microscopic channels is small compared to the mean free path of the gas molecules, i.e. the Knudsen number is too large, traditional fluid mechanics is no longer applicable [19]. Therefore, further adjustments are needed to apply this model to gas leakage.

6. SUMMARY AND OUTLOOK

In this paper, a simulation method based on Persson's theory to simulate the leakage of liquids through metallic seals has been presented and applied to gases. The simulation results have been compared to experiments. It was shown, that the simulation model overestimates the leakage up to a factor of ten. Therefore, it can be concluded, that the flow model used in the simulation does not apply to gases under the given conditions.

In future works, the flow used in this model must be adjusted for gases. For example, alternative flow

models based on the free molecular flow could be applied to this problem [9,19]. Further research is needed to describe the gas leakage accurately.

NOMENCLATURE

Acronyms

BFM	Bulk flow model
CFD	Computational fluid dynamics
ifas	Institute for fluid power drives and systems
PFAS	Per- and poly-fluoroalkyl substances
PFOA	Perfluorooctanoic acid
PSD	Power spectral density
PTFE	Polytetrafluoroethylene

Roman Symbols

a_C	1D contact area	m
$C(\boldsymbol{q})$	Surface roughness power spectrum	m^4
$C(q)$	Radially averaged $C(\boldsymbol{q})$	m^4
F	Normal force	N
$\dot{m}$	Mass flow rate	kg/s
p	Relative gas pressure	bar
p_C	Contact pressure	Pa
p_{max}	Exponential fitting parameter	Pa
R	Radius of the ball	m
R_S	Specific gas constant of air	J/K/kg
S_Q	Root mean square roughness	m
T	Temperature	K
t	Time	s
u	Average separation of surfaces	m
u_0	Exponential fitting parameter	m
V	Reference volume	m^3
$\boldsymbol{q}$	Surface roughness wave vector	1/m
q	Radial component of $\boldsymbol{q}$	1/m
x	Position on the slope of the seat	m
x_0	Location of the maximal contact pressure	m

Greek Symbols

γ	Peklenik number	1
ϕ_P	Pressure flow factor	1
ϕ_S	Shear flow factor	1
η	Viscosity	Pa s
ρ	Gas density	kg/m^3
θ	Angle of the slope of the seat	rad
Π	Ratio of the apparent and the real contact area	1
ζ	Magnification	1/m

REFERENCES

[1] Persson BNJ. Contact mechanics for randomly rough surfaces. Surface Science Reports

2006;61(4):201–27.

[2] Yamabe J, Nishimura S. Hydrogen-induced degradation of rubber seals 2018:769–816.

[3] Domingo JL, Nadal M. Human exposure to per- and polyfluoroalkyl substances (PFAS) through drinking water: A review of the recent scientific literature. Environ Res 2019;177:108648.

[4] European Chemicals Agency. Annex XV Restriction Report: Per- and polyfluoroalkyl substances (PFASs); Available from: https://echa.europa.eu/documents/10162/f605d4b5-7c17-7414-8823-b49b9fd43aea (5 July 2023).

[5] Fischer F, Schmitz K, Tiwari A, Persson BNJ. Fluid Leakage in Metallic Seals. Tribology Letters 2020;68(4):1–11.

[6] Persson BNJ. Leakage of metallic seals: role of plastic deformations. Tribology Letters 2016;63(3):42.

[7] Zhang Q, Chen X, Huang Y, Chen Y. Fractal modeling of fluidic leakage through metal sealing surfaces. AIP Advances 2018;8(4).

[8] Tikhomorov VP, Gorlenko OA, Izmerov MA. Simulation of leakage through mechanical sealing device. IOP Conf. Ser.: Mater. Sci. Eng. 2018;327:42047.

[9] Huon C, Tiwari A, Rotella C, Mangiagalli P, Persson BNJ. Air, Helium and Water Leakage in Rubber O-ring Seals with Application to Syringes. Tribol Lett 2022;70(2).

[10] Persson BNJ. Theory of rubber friction and contact mechanics. The Journal of Chemical Physics 2001;115(8):3840–61.

[11] Persson BNJ. Relation between interfacial separation and load: a general theory of contact mechanics. Phys Rev Lett 2007;99(12):125502.

[12] Lorenz B, Persson BNJ. Leak rate of seals: Effective-medium theory and comparison with experiment. The European Physical Journal E 2010;31(2):159–67.

[13] Persson BNJ. Interfacial fluid flow for systems with anisotropic roughness. Eur Phys J E Soft Matter 2020;43(5):25.

[14] Angerhausen J, Woyciniuk M, Murrenhoff H, Schmitz K. Simulation and Experimental Validation of Translational Hydraulic Seal Wear. Tribology International 2019;(123):296–307.

[15] Welch P. The use of fast Fourier transform for the estimation of power spectra: A method based on time averaging over short, modified periodograms. IEEE Trans. Audio Electroacoust. 1967;15(2):70–3.

[16] Scaraggi M, Angerhausen J, Dorogin L, Murrenhoff H, Persson BNJ. Influence of anisotropic surface roughness on lubricated rubber friction: Extended theory and an application to hydraulic seals. Wear 2018;410-411:43–62.

[17] Patir N, Cheng HS. Application of Average Flow Model to Lubrication Between Rough Sliding Surfaces. Journal of Lubrication Technology 1979;101(2):220–9.

[18] Persson BNJ, Scaraggi M. Lubricated sliding dynamics: flow factors and Stribeck curve. Eur Phys J E Soft Matter 2011;34(10):113.

[19] Antman SS, Marsden JE, Sirovich L. Microflows and Nanoflows. New York: Springer-Verlag; 2005.